

ISS-CREAM detector performance and tracking algorithms

Kenichi Sakai,^{a,b,*} Scott L. Nutter,^c Tyler Anderson,^d Yu Chen,^d Stephane Coutu,^d Tyler LaBree,^c Jason T. Link,^{a,b,†} John W. Mitchell,^b S. A. Isaac Mognet,^d Jacob Smith^{a,b} and Monong Yu^d

^aCenter for Research and Exploration in Space Science and Technology (CRESST), UMBC, Baltimore MD, 21250, USA

^bNASA Goddard Space Flight Center, Astroparticle Physics Laboratory, Greenbelt, MD 20771, USA

^cNorthern Kentucky University, Dept of Physics, Geology, and Engineering Technology, Highland Heights, KY 41099 USA

^dPenn State University, Department of Physics, University Park, PA 16802, USA

[†]No longer affiliated with NASA or CRESST as of May 2021.

E-mail: kenichi.sakai@nasa.gov

The goal of the ISS-CREAM experiment is to measure spectra of cosmic-ray particles up to 1000 TeV from protons to iron nuclei. The detector was designed to complement other current space-based cosmic-ray missions, and was installed on the ISS on August 22, 2017. During 539 days of on-orbit operations, ISS-CREAM recorded over 58 million events. The instrument consists of a 4-layer silicon charge detector, a tungsten/scintillating-fiber sampling calorimeter for energy measurement, top and bottom scintillating detectors to create a trigger, and a boronated scintillator detector for additional shower sampling. A variety of subsystem issues developed during on-orbit operations, requiring careful data filtering, the development of extensive calibrations, and multiple tracking algorithms. We report on the performance of the ISS-CREAM instrument and present details of the analysis.

37th International Cosmic Ray Conference (ICRC 2021)
July 12th – 23rd, 2021
Online – Berlin, Germany

*Presenter

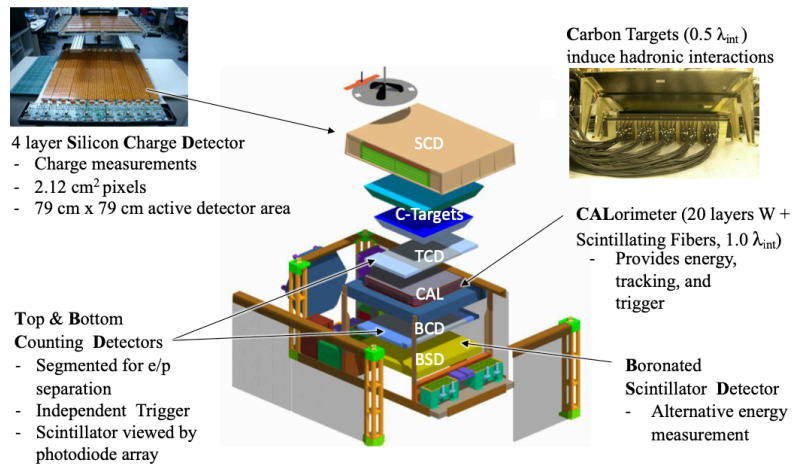


Figure 1: 3D view of ISS-CREAM instrument

1. Introduction

Direct measurements of the high-energy spectra of each species of cosmic-ray nuclei provide detailed insight into the general phenomenology of cosmic-ray acceleration and propagation in the Galaxy. Several features in the cosmic-ray spectrum have been identified, including the so-called knee at a few times 10^6 GeV, the second knee at a few times 10^8 GeV, and a spectral steepening above 10^{11} GeV. In addition to these famous features, PAMELA claimed the existence of an additional break in the proton spectrum at ~ 200 GeV[1]. This break was recently confirmed by many experiments like CREAM[2, 3], AMS-02[4], ATIC-2[5], CALET[6], and DAMPE[7], and was also observed in nuclei heavier than H (above ~ 200 GeV/n). This spectral hardening has not been understood yet, and is thought to be a good probe for modeling of the cosmic-ray transport properties in different regions of the Galaxy, a local effect of nearby supernova remnants, or reacceleration by weak shocks.

2. ISS-CREAM instrument

The ISS-CREAM experiment, illustrated in Fig. 1, grew out of a balloon-borne instrument, CREAM, which measures the fluxes of elements between protons and iron in an energy region nearly up to the knee[8]. As cosmic-ray nuclei enter the instrument from above in this expanded diagram, their charge is determined with multiple layers of a silicon detector, the SCD[9]. For some nuclei, a hadronic interaction takes place in the carbon targets, and the shower energy is measured in a 20 layer tungsten-scintillating fiber tracking calorimeter, or CAL. ISS-CREAM includes other detectors not flown on the balloon instrument. The Top and Bottom Counting Detectors, or TCD and BCD, are placed directly above and below the calorimeter, respectively, and give additional shower position measurements as well as providing an instrument trigger[10, 11]. A boronated scintillator

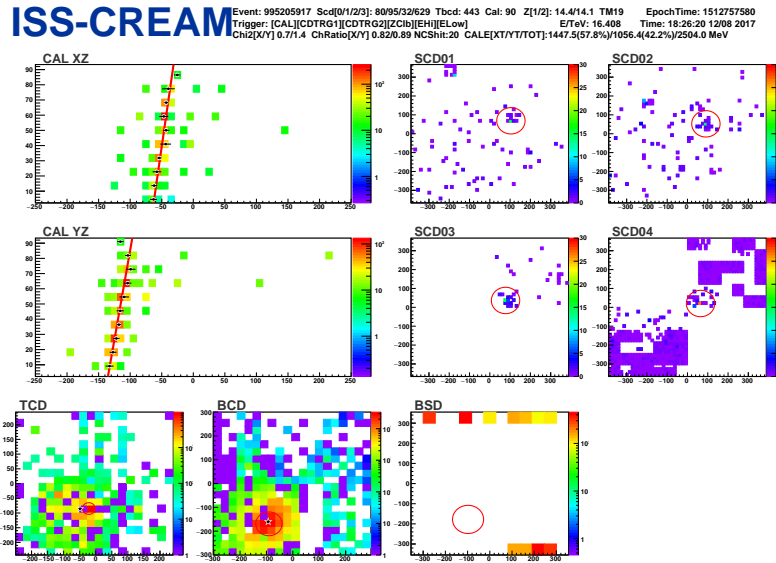


Figure 2: Event display of a typical high-energy event with a charge of 14 (Si)

detector, or BSD, located underneath the BCD, completes the detector stack, and provides an alternative energy measurement[12].

3. Event display

An event display was developed that enables simultaneous viewing of all detector responses. Figure 2 shows an example of a silicon event with reconstructible energy in the event display. This particular track was fitted to the mean energy-weighted CAL positions in each layer combined with the location of the pixels with the maximum signals in the TCD and BCD. The top CAL image shows a fit to the XZ view, and the bottom a fit to the YZ view. The two views are combined to provide a track and total visible energy deposition. Circles represent extrapolations of the track to other detectors with the circle size representative of position uncertainty. Some detectors have inefficient regions and noisy channels.

4. Detection efficiencies of each detector during observations

Figure 3 shows efficiencies of each detector operated during the science run. This science run was defined by the general high-voltage (HV) status of the CAL, and adds up to about 254 days. Channels that worked during the whole period of the science run have an efficiency of 100%. Half of the channels in 3 layers of the CAL have an efficiency of about 50%. The top two layers of the SCD operated well, but the bottom two SCD layers have low efficiency. In particular, SCD4 was extremely noisy and was turned off for much of the flight. Though the TCD was stable, the BCD had a dead zone near the center. In the BSD, 13 out of 18 photomultiplier tubes (PMTs) operated stably after a failure of the other 5 shortly after deployment to the ISS.

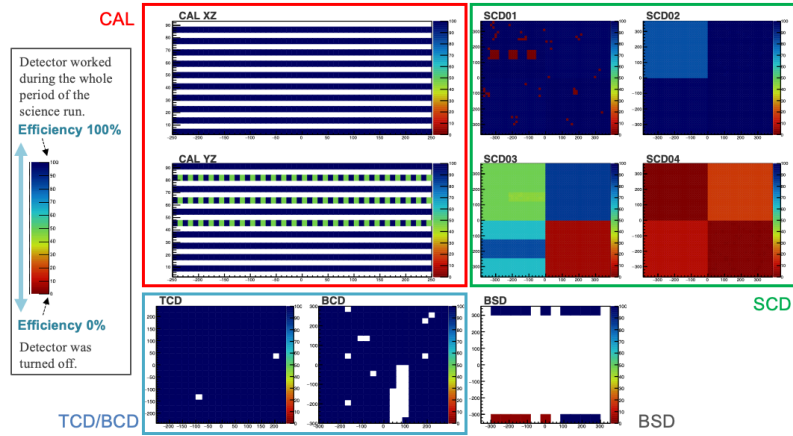


Figure 3: Detection efficiencies of each detector defined by HV status.

5. Detector noise characterization

A periodic calibration (CALIB) trigger provides an opportunity to measure detector noise spectra. It operated at a rate of 0.5 Hz and was subject to the same acquisition process as event data, making it ideal for background detector noise characterization. Various individual detector distributions, such as signal per channel and number of channels per event, were examined for CALIB events that did not also have a science trigger (from the CAL, or using the T/BCD), and were within good configuration periods. These noise distributions were not integrated into the simulations. Figure 4 shows SCD, T/BCD, and BSD/CAL channel noise distributions of CALIB trigger events in the top, middle and bottom panels, respectively, together with science trigger events as references. In SCD channels, noise signals can mimic a charge signature even beyond Fe. But such false charge signals are suppressed by requiring charge consistency between the top two layers of the SCD, and are mostly removed by using a combination of quality cuts in the SCD, T/BCD and BSD in the charge region above $Z=15$. The quality cut for the T/BCD (blue regions in Fig. 4 (middle)) required a signal above a threshold of

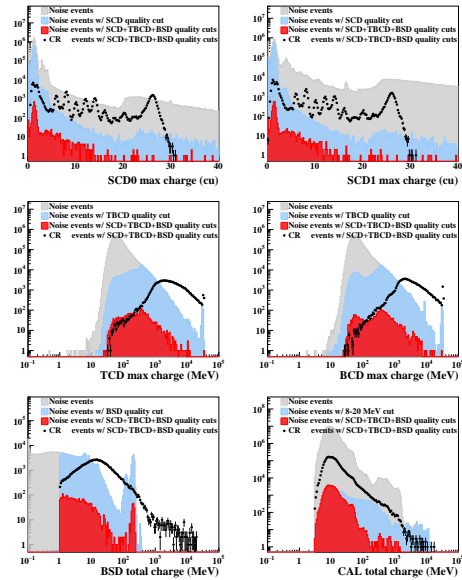


Figure 4: SCD (top), T/BCD (middle), BSD/CAL channel noise distributions in CALIB trigger events.

of

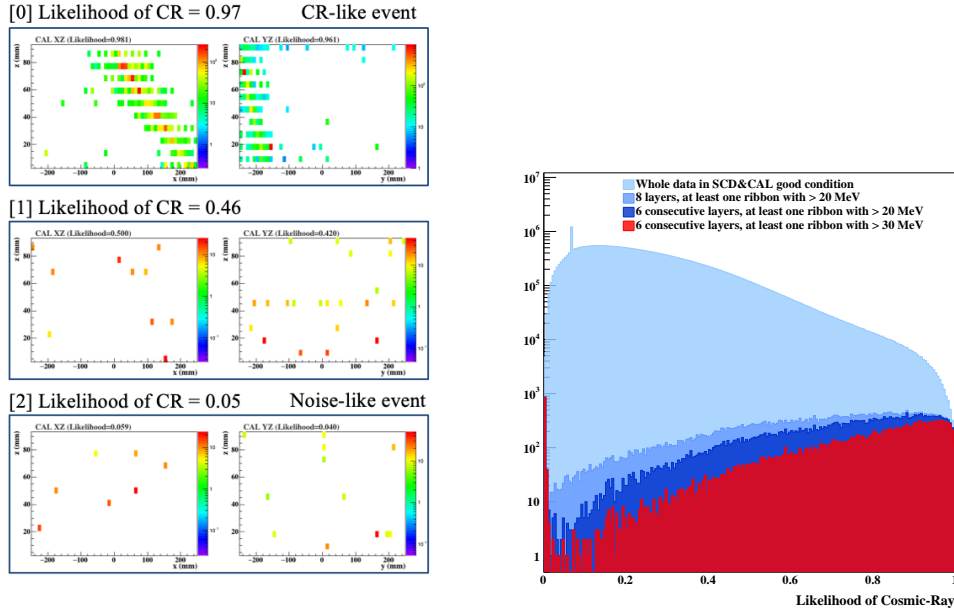


Figure 5: XZ and YZ views in the CAL for a cosmic-ray like event (top), a noise like event (bottom), and an in-between event (middle). **Figure 6:** Likelihood of an ob-orbit event being a true cosmic ray as determined by machine learning.

200 MeV: a quality cut for the BSD (blue regions in Fig. 4 (bottom, left)) required a signal above a threshold of 1 MeV. The quality cut for the CAL (blue region in Fig. 4 (bottom, right)) required 8 layers each with at least 20 MeV energy deposit showing great rejection power of noise events, but it's excluded from a combination of quality cuts. The reason is described in Section 6. To prevent the ambiguity in the absolute energy scale whose study is ongoing, the standard conversion factor 0.45MeV/ADC was used determined by the beam calibration without any tuning based on the on-orbit data.

6. Detector performance of the CAL

Figure 5 shows XZ and YZ views in the CAL for a cosmic-ray like event (top), a noise like event (bottom), and an in-between event (middle). These are categorized by using the on-orbit cosmic-ray likelihood as calculated by using a machine learning technique (TensorFlow)[13]. We eye-scanned cosmic-ray like events and noise events in the flight data and input them into TensorFlow as a training sample. Since we didn't use any track information, the likelihood is independent of the tracking method. Figure 6 shows the likelihood of an on-orbit event being a true cosmic ray (CR) as determined by machine learning. It indicates that the majority of triggered events are noise events, but we can select CR candidates by using typical quality cuts for shower events. The problem is statistics-related, as only 0.04 ~ 0.12% of events have useful hit information in the CAL.

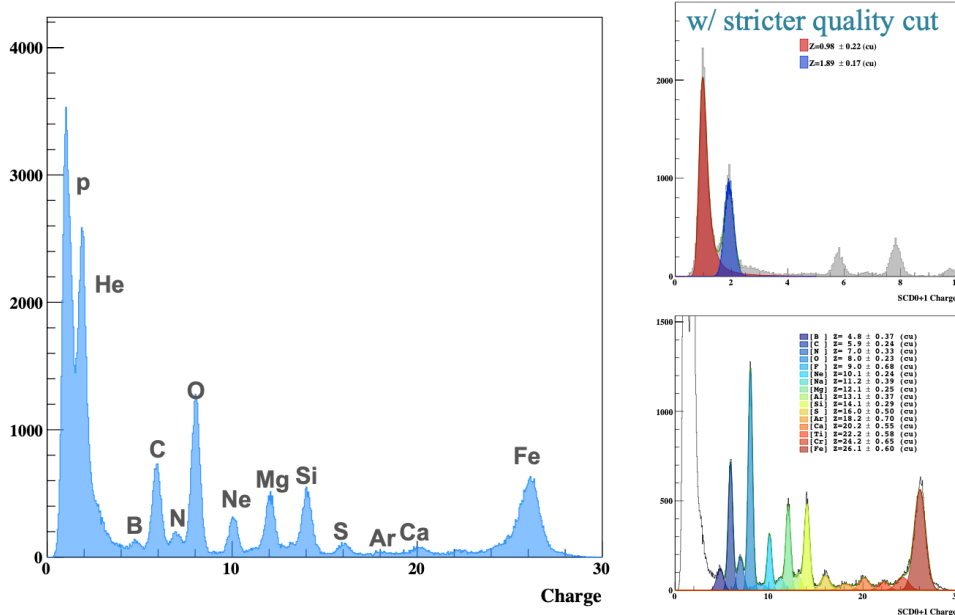


Figure 7: SCD charge distribution by using the average signal in the top two layers (left) based on new SCD/TCD/CAL-based tracking. Charge peak fits are shown for protons and helium (right top), and for Z from 6 to 26 (right bottom).

7. Tracking algorithms

The following two are picked up from 22 different tracking algorithms.

CAL-based tracking is the default and standard tracking method. Such a track is reconstructed by using energy-weighted CAL hits, then the SCD charge hit is searched for within a 70 mm radius of the extrapolated point. For most events, CAL tracking fails because more than 99.9% events don't have useful hit information in the CAL, as described in Section 6.

A new tracking algorithm was developed using the top two layers of the SCD, TCD and CAL hits, and was used for a preliminary flux calculation[14]. Even if the CAL is missing much data, the tracking can be reconstructed by using three points from the other detectors.

8. Detector performance of the SCD and T/BCD

8.1 SCD charge resolution

The measured charge distribution up to iron is shown in Fig. 7. The charge was determined by the average signal in the top two layers. Except for fits of the proton and helium charge peaks, the selection is very loose to get more iron statistics. The achieved charge resolution is 0.23 e for protons, and worsens with Z, up to 0.60 e for iron nuclei.

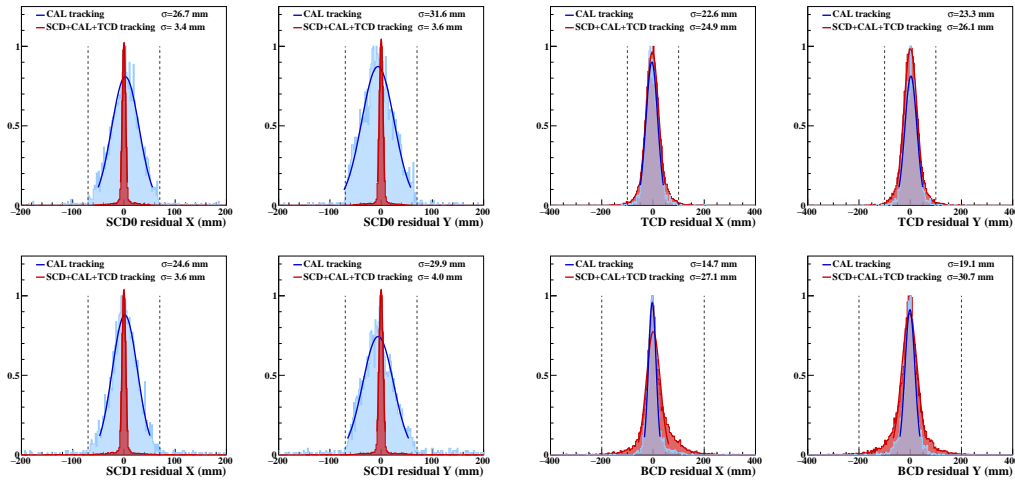


Figure 8: Position resolution of the SCD in XZ and YZ views. **Figure 9:** Position resolution of the T/BCD in XZ and YZ views.

8.2 Position resolution

Figures 8 and 9 show the position resolutions of the SCD and T/BCD. In each case, the blue histogram denotes the standard CAL-based tracking and position resolutions of each detector and seems to be reasonable. But the statistical sample of surviving events from the tracking quality cut criteria is small for CAL-based tracking, so that SCD/CAL/TCD-based tracking was used instead to calculate the preliminary fluxes[14].

9. Conclusions

The analysis of ISS-CREAM data is ongoing. Though there remain poorly understood aspects of the CAL performance, the other detectors have a more straightforward operational history on orbit and higher operational efficiency. With regards to the absolute energy of the CAL reconstruction, at least two different calibration methods were performed: (1) calibration using a BSD-based energy estimate by Yu Chen[15] and (2) calibration with a shower profile and machine learning analysis by Monong Yu[13]. Preliminary fluxes are reported by Scott L. Nutter[14].

Acknowledgements

This work was supported in the U.S. by NASA grants NNX17AB43G, NNX17AB42G, and their predecessor grants, as well as by directed RTOP funds to NASA GSFC. The authors also thank M. Geske, Penn State, for contributions to the BSD, and K. Wallace at Northern Kentucky University for contributions to Monte Carlo simulations. We also recognize the contributions of past CREAM and ISS-CREAM collaborators.

References

- [1] O. Adriani *et al.*, *Science* **332**, 69 (2011).

- [2] Y. S. Yoon *et al.*, *The Astrophysical Journal* **728**, 122 (2011).
- [3] Y. S. Yoon *et al.*, *The Astrophysical Journal* **839**, 5 (2017).
- [4] M. Aguilar *et al.*, *Phys. Rev. Lett.* **114**, 171103 (2015).
- [5] A. D. Panov *et al.*, *Bulletin of the Russian Academy of Sciences: Physics* **73**, 564 (2009).
- [6] O. Adriani *et al.* (CALET Collaboration), *Phys. Rev. Lett.* **122**, 181102 (2019).
- [7] Q. An *et al.*, *Science Advances* **5** (2019), 10.1126/sciadv.aax3793.
- [8] E. Seo *et al.*, *Advances in Space Research* **53**, 1451 (2014), cosmic Ray Origins: Viktor Hess Centennial Anniversary.
- [9] J. Lee *et al.*, *Astroparticle Physics* **112**, 8 (2019).
- [10] H. Hyun *et al.*, *Nucl. Inst. and Methods A* **787**, 134 (2015), new Developments in Photodetection NDIP14.
- [11] S. Kang *et al.*, *Advances in Space Research* **64**, 2564 (2019).
- [12] Y. Amare *et al.*, *Nucl. Inst. and Methods A* **943**, 162413 (2019).
- [13] M. Yu *et al.*, ICRC2021 Poster 476, these proceedings .
- [14] S. L. Nutter *et al.*, ICRC2021 Poster 696, these proceedings .
- [15] Y. Chen *et al.*, ICRC2021 Poster 866, these proceedings .